J. Fluid Mech. (1984), *vol.* 148, *pp.* 285–300
Printed in Great Britain

Nonlinear fluid motions in a container due to the discharge of an electric current

By O. O. AJAYI,
Engineering Analysis Unit, University of Lagos, Nigeria

C. SOZOU AND W. M. PICKERING
Department of Applied and Computational Mathematics, University of Sheffield, Sheffield, England

(Received 5 October 1983 and in revised form 16 June 1984)

The nonlinear electromagnetic stirring induced in a hemispheroidal container by the axisymmetric discharge of an electric current is investigated. The electric current is discharged into the fluid from a circular electrode which is at the centre of the equatorial plane of the container, the remaining part of the equatorial plane being a free surface. The equations of the problem are solved semi-analytically and results are presented for several sets of data. In the case of a point electrode when the current exceeds a critical value we have velocity breakdown. Here it is shown that, as the size of the area through which the current is discharged increases, the intensity of the flow field decreases, and thus for a larger electrode a larger amount of current can be discharged without velocity breakdown. When, however, the current is sufficiently large the solution becomes unstable, and this indicates velocity breakdown. Finally in an Appendix the solution for the case of a point discharge in a semi-infinite fluid is expressed in analytic (series) form.

1. Introduction

The motion of the molten metal in a weld pool determines the heat and mass transfer in it (Christensen, Davis & Gjermundsen 1965; Apps & Milner 1963) and consequently is an important factor in determining the chemical reactions between and the fusion of the metals being joined together. The experiments of Woods & Milner (1971), Kublanov & Erokhin (1974) and Butsenieks *et al.* (1976) have demonstrated that the fluid motions in the weld pool are primarily caused by electromagnetic forces and that the effect of these forces is conducive to the mixing process. A secondary cause of these motions is the plasma jet generated in the welding arc (Wienecke 1955; Milner, Salter & Wilkinson 1960). The theoretical study of these motions has attracted the attention of many authors; for example, Lundquist (1969), Shercliff (1970), Sozou (1971), Sozou & Pickering (1976) and Atthey (1980).

The early attempts to understand the role played by the Lorentz force in the welding process were concerned with situations in which the fluid extends to infinity and the current enters the fluid through a point source (Lundquist 1969; Sozou 1971; Shercliff 1970). This configuration is, of course, too idealized to successfully describe the practical welding situation, and so Sozou & Pickering (1976) considered the case where these flows take place in a finite container. They assumed that the container was a hemispherical bowl and the current entered the fluid through a point at the centre of the free surface of the fluid. The flow pattern predicted by the point source model is compatible with observations in the weld pool, but the predicted velocity

is too large and breaks down when the discharged current J_0 exceeds a certain critical value. In practice currents much in excess of the critical value of J_0 are passed through the weld pool, and no velocity breakdown occurs.

The dimensionless parameter $K = \chi J_0^2/2\pi^2\nu^2\rho$ plays a prominent role in the determination of these flows. Here χ, ν and ρ denote respectively the magnetic permeability, kinematic viscosity and density of the fluid, and J_0 the total current discharged in the fluid. The numerator of K is proportional to the electromagnetic force exerted on the fluid, and the denominator is a measure of the resistance put up by the fluid owing to its viscosity and density. With the parameter K we associate a geometrical factor which depends on the shape of the container and the distribution of the rotational part of the Lorentz force that drives the flow field. (The irrotational part of the Lorentz force is taken up by the fluid pressure and does not contribute to the flow field.) For a prescribed configuration the geometrical factor is specified; and, when K increases, the electromagnetic force on the fluid and the intensity of the flow increase and eventually the flow field breaks down. The quantitative discrepancy between theory and the weld-pool observations must be due to the assumed structure of the current discharge and the consequent increase in the rotational part of the Lorentz force (Sozou 1974).

Recent experiments by Boyarevich & Shcherbinin (1983) showed that, if the experimental arrangement matches the theoretical model, agreement between theory and observation concerning the critical value of J_0 is satisfactory. These authors discharged axisymmetrically an electric current J_0 from a small electrode at the centre of the plane end of a hemispherical container filled with mercury. They found that when J_0 exceeds 15 A the induced flow develops azimuthal instabilities. Boyarevich & Shcherbinin used an external magnetic field to study these instabilities, but that field can be produced only by a uniform distribution of magnetic poles covering the half of the axis of the container that terminates at the plane end and does not penetrate the hemisphere.

The theoretical flow patterns associated with the electrically driven flows can be made slower and thus quantitatively correlate better with the observed flows in weld pools by reducing the rotational part of the Lorentz force acting on the fluid. One approach, employed by Andrews & Craine (1978), is to model situations which occur in welding by a distribution of sources and sinks situated outside the fluid region. They considered the steady axisymmetric slow viscous flow induced in a hemispherical container due to various idealized axisymmetric representations of the current sources and found that by varying the current distribution within the fluid the general flow pattern is qualitatively altered. Atthey improved on the idea of Andrews & Craine; he assumed a distribution of current that enabled a large amount of current to flow in the direction of the axis of symmetry and also retained the inertia terms in the momentum equation. Craine & Weatherill (1980) studied configurations similar to those considered by Andrews & Craine and by Atthey, but with the addition of a uniform external magnetic field parallel to the pool axis. That configuration is associated with meridional flow and azimuthal swirl.

In order to exclude the effects of the plasma jet, the effects of the current flow through the molten metal are sometimes simulated by an electrode touching the surface of the pool, e.g. by Kublanov & Erokhin (1974). Sozou & Pickering (1978, subsequently referred to as SP) considered a model which resembles that studied by Kublanov & Erokhin. These authors investigated the Stokes flow field generated in a hemispheroidal container by the axisymmetric discharge of an electric current into the fluid through a circular electrode which is situated at the centre of the equatorial

plane of the spheroid. The neglect of the inertial forces in their analysis makes their solution valid only for low currents. At high currents the contribution of the nonlinear effects is likely to be significant and even cause velocity breakdown, and the terms representing the nonlinearities must be retained in the governing equations. It is our aim to consider the effects of these nonlinear terms for various electrode sizes in this paper. Atthey and Craine & Wetherill did not report a velocity breakdown for the models they considered, but this is probably due to the fact that they did not use a sufficiently large current.

Over the years some queries have been raised privately about the breakdown point of the original solution constructed by Sozou (1971) concerning the flow field generated by a current source. Recently Boyarevich (1981) studied the analytic properties of equations associated with the flow field of a current source and various boundary conditions by means of matched asymptotic expansions. However, this is not necessary for the original case studied by Sozou (1971). The solution constructed for that case can be expressed in terms of power series. This is done in Appendix B, and the originally noted velocity breakdown is reconfirmed.

2. Formulation of the problem

We consider an oblate axisymmetric hemispheroidal bowl full of an incompressible conducting fluid of density ρ and kinematic viscosity ν such that the plane boundary of the fluid forms a free surface, except for a circular electrode of radius k whose centre is coincident with the centre of the equatorial plane of the hemispheroid. The semimajor and semiminor axes of the bowl are a and c, respectively. It is convenient to use oblate spheroidal coordinates (μ, ζ, ϕ), which are related to the cylindrical polar coordinates (x, ϖ, ϕ) by

$$x = k\mu\zeta, \quad \varpi = k(1-\mu^2)^{\frac{1}{2}}(\zeta^2+1)^{\frac{1}{2}}, \quad \phi = \phi \quad (-1 \leqslant \mu \leqslant 1,\ 0 \leqslant \zeta \leqslant \infty,\ 0 \leqslant \phi \leqslant 2\pi).$$

The origin is at the centre of the circular electrode, and the positive x-axis points into the fluid along the axis of symmetry. The bowl surface is given by $\zeta = \zeta_0$, $1 \geqslant \mu \geqslant 0$; the electrode is described by $\zeta = 0$, $0 \leqslant \mu \leqslant 1$; and the free surface is given by $\mu = 0$, $0 < \zeta \leqslant \zeta_0$. The parameters a, c, k and ζ_0 are related by $a = k(\zeta_0^2+1)^{\frac{1}{2}}$, $c = k\zeta_0$. Large values of ζ_0, say $\zeta_0 \gg 1$, are associated with a small electrode ($a \ll k$) and a nearly spherical container ($a/c \approx 1$), and small values of ζ_0, say $\zeta_0 \ll 1$, correspond to a large electrode ($a \approx k$) and a relatively shallow container ($a \gg c$). Note that the free surface area is πc^2.

We suppose that the electrode is raised to a certain potential, thus allowing an electric current to flow into the fluid. (The conductivity of the region $\mu > 0$ is σ, a constant, and the conductivity of the region $\mu < 0$ is assumed zero.) This configuration is clearly axisymmetric. We assume that the electromotive force induced by the motion of the fluid is negligible. Then the equation of the current lines is given by $\mu =$ constant. If the total current discharged into the fluid is J_0, the electrostatic potential $\boldsymbol{\Phi}$ and the current density $\boldsymbol{j}$ are given by

$$\boldsymbol{\Phi} = \frac{J_0 \cot^{-1}\zeta}{2\pi k\sigma}, \tag{1}$$

$$\boldsymbol{j} = -\sigma\nabla\boldsymbol{\Phi} = \frac{J_0}{2\pi k^2(\zeta^2+\mu^2)^{\frac{1}{2}}(\zeta^2+1)^{\frac{1}{2}}}\boldsymbol{e}_\zeta. \tag{2}$$

Figure 1 shows an axial section of the configuration studied for the case $\zeta_0 = 1$.

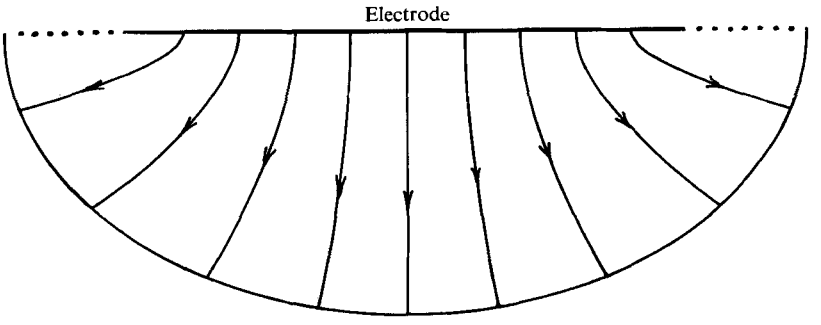

FIGURE 1. Axial section of the hemispheroidal bowl for the case $\zeta_0 = 1$. The curves show the direction of current flow corresponding to the case where the electrode is at a fixed potential. The dotted lines represent the free surface.

On integrating the equation $\nabla \times \boldsymbol{B} = \chi \boldsymbol{j}$, where χ is the magnetic permeability of the medium, we find that the associated magnetic induction $\boldsymbol{B}$ is given by

$$\boldsymbol{B} = \frac{\chi J_0 (1-\mu)}{2\pi k (\zeta^2+1)^{\frac{1}{2}} (1-\mu^2)^{\frac{1}{2}}} \boldsymbol{e}_\phi. \tag{3}$$

The steady momentum equation governing our problem is

$$-\rho \boldsymbol{v} \times \operatorname{curl} \boldsymbol{v} = -\nabla(p + \tfrac{1}{2}\rho v^2) + \nu\rho \nabla^2 \boldsymbol{v} + \boldsymbol{j} \times \boldsymbol{B}, \tag{4}$$

where p is the pressure and $\boldsymbol{v}$ the fluid velocity. In view of the axisymmetric nature of the problem we may satisfy the equation of continuity by introducing a stream function ψ such that

$$\boldsymbol{v} = \frac{\boldsymbol{e}_\mu}{k^2(\zeta^2+\mu^2)^{\frac{1}{2}}(1-\mu^2)^{\frac{1}{2}}} \frac{\partial \psi}{\partial \zeta} - \frac{\boldsymbol{e}_\zeta}{k^2(\zeta^2+\mu^2)^{\frac{1}{2}}(\zeta^2+1)^{\frac{1}{2}}} \frac{\partial \psi}{\partial \mu}. \tag{5}$$

It is convenient to introduce dimensionless variables z and Ψ, defined by

$$\zeta = \zeta_0 z, \quad \psi = \nu c K \Psi, \tag{6), (7}$$

where $K = \chi J_0^2 / 2\pi^2 \nu^2 \rho$. The surface of the bowl is now given by $z = 1$.

Taking the curl of (4) and using (2), (3) and (5)–(7), after some algebra we obtain

$$\mathrm{D}^2\left[\frac{\mathrm{D}^2\Psi}{z^2+\zeta_0^{-2}\mu^2}\right] + K\left\{(z^2+\zeta_0^{-2})\frac{\partial \Psi}{\partial \mu}\frac{\partial}{\partial z}\left[\frac{\mathrm{D}^2\Psi}{(z^2+\zeta_0^{-2}\mu^2)(z^2+\zeta_0^{-2})}\right] - (1-\mu^2)\frac{\partial \Psi}{\partial z}\frac{\partial}{\partial \mu}\left[\frac{\mathrm{D}^2\Psi}{(1-\mu^2)(z^2+\zeta_0^{-2}\mu^2)}\right]\right\} = \frac{z(1-\mu)}{z^2+\zeta_0^{-2}}, \tag{8}$$

where

$$\mathrm{D}^2 = (z^2+\zeta_0^{-2})\frac{\partial^2}{\partial z^2} + (1-\mu^2)\frac{\partial^2}{\partial \mu^2}.$$

The boundary conditions for the solution of (8) are zero velocity on the electrode and the surface of the bowl, i.e. at $z = 0$ and $z = 1$. At the free surface, i.e. on $\mu = 0$, the normal component of $\boldsymbol{v}$ and the shear stress are zero. If $\Psi = \Psi(\mu, z)$ these conditions require that

$$\Psi(\mu, 0) = 0, \quad \Psi_z(\mu, 0) = 0, \tag{9), (10}$$

$$\Psi(\mu, 1) = 0, \quad \Psi_z(\mu, 1) = 0, \tag{11), (12}$$

$$\Psi(0, z) = 0, \quad \Psi_{\mu\mu}(0, z) = 0. \tag{13), (14}$$

We set
$$\Psi = \sum_{n=1}^{\infty} F_n(z)\, I_{2n+1}(\mu), \tag{15}$$

where
$$I_{2n+1} = \frac{P_{2n-1}(\mu) - P_{2n+1}(\mu)}{4n+1} = \frac{(1-\mu^2)\, P'_{2n}(\mu)}{2n(2n+1)}, \tag{16}$$

and P_m is the Legendre polynomial of degree m. Here and in subsequent expressions a prime denotes differentiation with respect to the argument of the function. Since $P_{2n+1}(0) = I_{2n+1}(0) = I''_{2n+1}(0) = 0$, this form of Ψ satisfies (13) and (14) automatically, and (9)–(12) will be satisfied if

$$F_n(0) = 0, \quad F'_n(0) = 0, \quad F_n(1) = 0, \quad F'_n(1) = 0. \tag{17)–(20}$$

Note that (15) and (16) imply that on the axis of symmetry $\mu = 1$, $\Psi = 0$ and v (see (5)) is finite.

On substituting (15) in (8) and making use of the equation

$$(1-\mu^2)\, I''_{2n+1} + 2n(2n+1)\, I_{2n+1} = 0,$$

after some manipulation, we obtain

$$\begin{aligned}
\sum_{m=1}^{\infty} \Big\{ & \{(\zeta_0^2 z^2 + 1)\,[(z^2 + \zeta_0^{-2}\mu^2)\, G''_m - 4z G'_m] - 2[(2m+3)(m-1)(\zeta_0^2 z^2 + \mu^2) \\
& + 6\mu^2 - 2]\, G_m\}\, I_{2m+1} - 4\mu(1-\mu^2)\, G_m\, I'_{2m+1} \\
& + K F_m\, I'_{2m+1} \sum_{s=1}^{\infty} [(\zeta_0^2 z^2 + \mu^2)\, G'_s - \frac{2\zeta_0^2 z}{\zeta_0^2 z^2 + 1}(2\zeta_0^2 z^2 + \mu^2 + 1)\, G_s]\, I_{2s+1} \\
& - K F'_m\, I_{2m+1} \sum_{s=1}^{\infty} [(\zeta_0^2 z^2 + \mu^2)\, I'_{2s+1} + \frac{2\mu}{1-\mu^2}(\zeta_0^2 z^2 + 2\mu^2 - 1)\, I_{2s+1}]\, G_s \Big\} \\
& = \frac{z}{\zeta_0^2 z^2 + 1}(\zeta_0^2 z^2 + \mu^2)^2 (1-\mu),
\end{aligned} \tag{21}$$

where
$$G_s = (z^2 + \zeta_0^{-2})\, F''_s - 2s(2s+1)\, F_s. \tag{22}$$

The functions G_s and the fluid vorticity $\nabla \times v$ are connected by the equation

$$\nabla \times v = -\frac{\nu K \sum_{n=1}^{\infty} G_n(z)\, I_{2n+1}(\mu)}{c^2(\zeta^2 + \zeta_0^{-2}\mu^2)(z^2 + \zeta_0^{-2})^{\frac{1}{2}}(1-\mu^2)^{\frac{1}{2}}} e_\phi. \tag{23}$$

The analysis so far, apart from a slight change in notation, is similar to that employed by SP. Our equation (21) corresponds to (24) in the paper by SP, where the nonlinear terms represented by the coefficient of K in (21) were neglected.

If we multiply (21) by $I_{n+1}(\mu)/(1-\mu^2)$ and integrate both sides of the resulting equation with respect to μ over the interval $(0, 1)$, after some algebra we obtain

$$\begin{aligned}
& a_1 G''_n + a_2 G'_n + a_3 G_n + a_4 G''_{n+1} + a_5 G_{n+1} + a_6 G''_{n-1} + a_7 G_{n-1} \\
& \qquad + K \sum_{m=1}^{\infty} \sum_{s=1}^{\infty} [F_m(a_8 G'_s + a_9 G_s) + a_{10} F'_m G_s] = a_{11},
\end{aligned} \tag{24}$$

where $a_1, \ldots, a_7$ and a_{11} are functions of ζ_0, n and z, and a_8, a_9 and a_{10} are functions of ζ_0, m, n, s and z. These functions are given in Appendix A.

The two solutions associated with the complementary function of (22), say $f_{s1}(z)$ and $f_{s2}(z)$, are given by

$$f_{s1}(z) = (z^2+\zeta_0^{-2})\,p'_{2s}(\zeta_0 z), \quad f_{s2}(z) = (z^2+\zeta_0^{-2})\,q'_{2s}(\zeta_0 z),$$

where
$$f_{s1}(z)\,f'_{s2}(z) - f'_{s1}(z)\,f_{s2}(z) = 2s(2s+1)\,\zeta_0^{-3}. \tag{25}$$

Here we have used Lamb's (1932, p. 143) notation, that is

$$p_{2s}(t) = (-)^s P_{2s}(\mathrm{i}t), \quad q_{2s}(t) = (-)^s\,\mathrm{i}Q_{2s}(\mathrm{i}t),$$

where $Q_m(x)$ denotes the Legendre function of the second kind of order m. If we multiply (22) by f_{si} $(i = 1, 2)$ and integrate, we obtain

$$f_{s1}(z)\,F'_s(z) - f'_{s1}(z)\,F_s(z) = \int_{bs_1}^{z} p'_{2s}(\zeta_0 x)\,G_s(x)\,\mathrm{d}x, \tag{26}$$

$$f_{s2}(z)\,F'_s(z) - f'_{s2}(z)\,F_s(z) = \int_{bs_2}^{z} q'_{2s}(\zeta_0 x)\,G_s(x)\,\mathrm{d}x. \tag{27}$$

Since $F_s(0) = F'_s(0) = 0 = F_s(1) = F'_s(1)$, we set $b_{s1} = b_{s2} = 0$ and

$$\int_0^1 p'_{2s}(\zeta_0 x)\,G_s(x)\,\mathrm{d}x = 0, \quad \int_0^1 q'_{2s}(\zeta_0 x)\,G_s(x)\,\mathrm{d}x = 0. \tag{28), (29}$$

If we eliminate F'_s between (26) and (27) and make use of (25), after some slight rearrangement, we obtain

$$F_s(z) = \frac{\zeta_0(\zeta_0^2 z^2+1)}{2s(2s+1)} \int_0^z G_s(x)\,[p'_{2s}(\zeta_0 x)\,q'_{2s}(\zeta_0 z) - p'_{2s}(\zeta_0 z)\,q'_{2s}(\zeta_0 x)]\,\mathrm{d}x. \tag{30}$$

Equations (28) and (29) are the boundary conditions for G_s. When the functions G_s are known Ψ is constructed from (15) and (30).

The approach adopted here can easily be modified to accommodate the case where the solid electrode ($z = 0$, $0 \leqslant \mu \leqslant 1$) is replaced by a free surface where the shear stress is zero. In that case the condition $\Psi_z(0, \mu) = 0$ is replaced by $\Psi_{zz}(0, \mu) = 0$ and, in view of the assumed form of Ψ, (18) is replaced by $F''_n(0) = 0$. Since $f_{s1}(0) = 0$, to satisfy the conditions $F_s(0) = F_s(1) = F'_s(1) = 0$, we set $b_{s1} = 0$, $b_{s2} = 1$ and impose (28). Equation (22) and the conditions $F_s(0) = F''_s(0) = 0$ imply that

$$G_s(0) = 0.$$

The equation $G_s(0) = 0$ replaces (29) as one of the boundary conditions of the problem. If we then eliminate F'_s between (26) and (27) (with $b_{s1} = 0$, $b_{s2} = 1$) we obtain

$$F_s(z) = \frac{\zeta_0(\zeta_0^2 z^2+1)}{2s(2s+1)} \left[q'_2(\zeta_0 z) \int_0^z G_s(x)\,p'_{2s}(\zeta_0 x)\,\mathrm{d}x + p'_{2s}(\zeta_0 z) \int_z^1 G_s(x)\,q'_{2s}(\zeta_0 x)\,\mathrm{d}x \right].$$

A different current input into the fluid, through $z = 0$, $0 \leqslant \mu \leqslant 1$, is also possible. A change in the structure of current flow will change the function a_{11}. The numerical solution described in §§3 and 4 was restricted to the case of a solid electrode and the current density given by (2).

3. The numerical method

It is obvious that (22) and (24) must be solved by an iterative process. First we assume that the functions $F_n(z)$ are known and solve (24) for the functions $G_n(z)$; these results are then used to obtain a new approximation to $F_n(z)$ using (30). This process is continued until convergence is obtained; here we assume that there is convergence when two successive iterations produced the same output to the third significant figure for all G_n at all mesh points. The infinite series (15) was truncated at N terms, that is we set $F_n(z) = G_n(z) = 0$ for all $n > N$.

To solve the set of equations (24) we divided the interval $(0, 1)$ into M equal parts and numbered the nodal points from 1 to $M+1$, with the point 1 corresponding to the point $z = 0$ and the point $M+1$ corresponding to $z = 1$. We used central differences to approximate the derivatives in (24). For a specified n (24) was evaluated at the nodal points $2, \ldots, M$, thus generating $M-1$ linear equations. Equations (28) and (29) were then evaluated using the trapezoidal rule, and these contributed two more equations giving a total of $M+1$ equations, which were solved for all the functions

$$G_n(z) \quad (n = 1, 2, 3, \ldots, N).$$

The general procedure adopted for constructing the solution is as follows. For a given ζ_0 we solved the linear problem, where the inertia terms in the momentum equation are ignored, that is we set $a_8 = a_9 = a_{10} = 0$. It may be noted that an iterative process is not needed when the flow field is linear. We then prescribed a relatively low value to K and solved the nonlinear problem iteratively, using as the initial approximation to $F_n(z)$ the values obtained for the linear problem. This solution was stored in a file and used as a first approximation for computing a solution for a higher value of K. The process was repeated with an increased value of K, using as initial approximations to $F_n(z)$ for the higher K the values corresponding to the last K.

For relatively low K, depending on ζ_0, the process described here converges rapidly, but as K increases more iterations are required for convergence, and eventually a stage is reached where convergence is practically impossible, even if we use a small relaxation factor. Examination of our computer output showed that, excepting the endpoints, $F_1(z) > 0$ and, for $n \neq 1$, $F_n(z)$ may change sign. In the linear case $F_1(z) \gg |F_n(z)|$. As K increases, the amplitude of $F_1(z)$ decreases and, in general, that of $F_n(z)$ increases. This implies that when K increases sufficiently we must increase the number of terms N used in the series representation for Ψ. Gradually $|F_2(z)|$ and then $|F_3(z)|$ and so on exceed $F_1(z)$ for some z, and eventually the system of equations set up becomes unstable. The numerical instability starts near the origin, where the rate of decrease of F_1, as K increases, is maximum. The increase in the amplitude of $F_n(z)$ for $n \neq 1$ and the instability indicate that, when K is sufficiently large for a particular ζ_0, the series (15) diverges, that is, we have velocity breakdown as originally suggested by Sozou (1971) for the case of a point electrode in a semi-infinite fluid. In practice we fixed ζ_0, determined $N(\zeta_0)$ and carried out computations for increasing values of K. The results, which are presented in §4, refer to cases where

$$F_1(z) \gg |F_N(z)|. \tag{31}$$

For a given ζ_0, when (31) was violated or instability occurred we terminated our computations and did not attempt to establish an upper limit (which is difficult) to K. For $\zeta_0 = 100$, for instance, we find that (31) is satisfied when $K \leqslant 80$, but when $K = 120$ the system of equations is unstable. The results presented for $\zeta_0 = 100$ refer

to $K \leqslant 80$. Since $|P_m(\mu)| \leqslant 1$, (15) and (16) indicate that when (31) is satisfied the approximation of Ψ by the first N terms of (15) gives a reasonably accurate representation for the stream function.

4. Results and discussion

We carried out computations for $\zeta_0 = 0.5$, 1, 10 and 100. To start with we looked into the problem of the number of terms to be retained in the series for Ψ in order to accurately evaluate the flow field. We found that the larger the value of ζ_0 the more rapid is the decrease in the magnitude of $F_n(z)$ as n increases. Thus, for a certain accuracy in the evaluation of Ψ fewer terms are needed as ζ_0 increases. After some test trials we decided to set $N = 12$ for $\zeta_0 = 0.5$, $N = 7$ for $\zeta_0 = 1$ and for $\zeta_0 = 10$ and $N = 5$ for $\zeta_0 = 100$. We chose a steplength $\delta z = 0.025$ for all ζ_0 considered. Some of our results are shown in tables 1 and 2 and in figures 2–4.

Since $I'_{2n+1}(1) = -1$, (5)–(7) and (15) imply that the velocity u along the axis $\mu = 1$ is given by

$$u = \frac{\nu K}{c(z^2 + \zeta_0^{-2})} \sum_{n=1}^{N} F_n(z). \tag{32}$$

Tables 1 and 2 show values of u for the cases $\zeta_0 = 100$, 10, 1 and 0.5 and for various values of K. The linear case refers to the Stokes-flow problem where the inertia terms are ignored, that is to cases where the coefficient of K in (24) is set equal to zero. The corresponding Stokes-flow problem was also considered by SP, who used a lower N and a slightly different procedure to evaluate $F_n(z)$. Our u for the linear case is a little larger near $z = 0$ and a little smaller near $z = 1$ than the corresponding u obtained by SP.

In the discussion presented below it is convenient to assume that the depth c of the container is kept constant and express the various scale lengths in terms of c and the parameter ζ_0. We recall that $c = k\zeta_0$ and the free surface area is $\pi(a^2 - k^2) = \pi c^2$. The maximum value of ψ, say ψ_m, associated with a particular set of data is a measure of the overall intensity of the flow field. Inspection of the data of figures 2 and 4 shows that, in the Stokes-flow regime when ζ_0 decreases from 100 to 0.5, ψ_m decreases by more than two orders of magnitude (from about $6 \times 10^{-3} K/\nu c$ to about $10^{-5} K/\nu c$). For a particular K, the change in the intensity of the flow, as ζ_0 varies, depends on the following reasons.

(i) The value of the parameter R = curved surface/volume, of the hemispheroid. Since the curved surface due to frictional effects slows down v, an increase in R must correspond to a reduction in the intensity of the flow. It can be shown that, when ζ_0 decreases from 100 to 0.5, R increases by a factor of 1.5 and this cannot be the main cause for the decrease in ψ_m, for the Stokes-flow problem, by a factor of nearly three orders of magnitude.

(ii) The size of the area of the electrode surface $\pi c^2 \zeta_0^{-2}$ which, owing to frictional effects, slows down the overall velocity field. An indication of the frictional effects of the electrode is provided by the configurations considered in Appendix B, that is by the flow fields generated by an electric discharge in a semi-infinite fluid from a point of the plane bounding the fluid. When the boundary is a free surface the nonlinear flow breaks down at $K = 94.1$, and when the free surface is replaced by a wall (which slows down the velocity field) the flow breaks down at $K = 300.1$. It can also be shown that, in the corresponding Stokes-flow regime,

$$u = \frac{\nu K(0.5 \log 2 - 0.25)}{r} \approx \frac{0.097 \nu K}{r}$$

	$\zeta_0 = 100$			$\zeta_0 = 10$		
z	linear case	$K = 40$	$K = 80$	linear case	$K = 500$	$K = 1000$
0.1	9.11, −1	1.32, 0	1.50, 0	1.40, −1	1.06, −1	8.65, −2
0.2	4.30, −1	6.42, −1	7.78, −1	1.67, −1	1.49, −1	1.23, −1
0.3	2.57, −1	4.01, −1	5.27, −1	1.34, −1	1.46, −1	1.24, −1
0.4	1.63, −1	2.65, −1	3.82, −1	9.73, −2	1.34, −2	1.17, −1
0.5	1.03, −1	1.73, −1	2.76, −1	6.60, −2	1.19, −1	1.08, −1
0.6	6.19, −2	1.07, −1	1.87, −1	4.13, −2	1.00, −1	9.60, −2
0.7	3.32, −2	5.87, −2	1.12, −1	2.28, −2	7.69, −2	8.03, −2
0.8	1.43, −2	2.58, −2	5.30, −1	9.96, −3	4.72, −2	5.74, −2
0.9	3.50, −3	6.48, −3	1.42, −2	2.47, −3	1.58, −2	2.43, −2

TABLE 1. Values of $cu/\nu K$ for some ζ_0 and K

	$\zeta_0 = 1$			$\zeta_0 = 0.5$		
z	linear case	$K = 5 \times 10^4$	$K = 10^5$	linear case	$K = 10^5$	$K = 10^6$
0.1	7.82, −5	3.35, −5	1.89, −5	1.88, −6	1.74, −6	9.20, −7
0.2	2.45, −4	1.15, −4	6.72, −5	6.09, −6	5.71, −6	3.19, −6
0.3	4.11, −4	2.14, −4	1.29, −4	1.07, −5	1.02, −5	6.03, −6
0.4	5.18, −4	3.00, −4	1.87, −4	1.43, −5	1.38, −5	8.66, −6
0.5	5.34, −4	3.51, −4	2.24, −4	1.57, −5	1.54, −5	1.03, −5
0.6	4.64, −4	3.53, −4	2.32, −4	1.45, −5	1.45, −5	1.04, −5
0.7	3.33, −4	2.99, −4	2.06, −4	1.11, −5	1.13, −5	8.72, −6
0.8	1.81, −4	1.92, −4	1.40, −4	6.44, −6	6.58, −6	5.47, −6
0.9	5.40, −5	6.57, −5	5.04, −5	2.02, −6	2.08, −6	1.84, −6

TABLE 2. Values of $cu/\nu K$ for some ζ_0 and K

when the boundary is a free surface, and when the boundary is a wall

$$u = \frac{\nu K(1.5 \log 2 - 1)}{r} \approx \frac{0.040 \nu K}{r},$$

where r is the distance from the discharge. Thus when the free surface is replaced by a wall u is reduced by a factor ≈ 2.4. The data of tables 1 and 2 show that, in the linear regime when ζ_0 decreases from 100 to 0.5, u decreases by several orders of magnitude, and therefore the frictional effects of the electrode cannot be the main cause in the reduction of u (as ζ_0 is reduced from 100 to 0.5).

(iii) The agent generating the velocity field, that is the rotationality of the Lorentz force given by

$$\nabla \times (\boldsymbol{j} \times \boldsymbol{B}) = \frac{Kz}{c^4(1+\mu)(z^2+\zeta_0^{-2})^{\frac{3}{2}}(z^2+\zeta_0^{-2}\mu^2)} \boldsymbol{e}_\phi. \tag{33}$$

The mean value of $\nabla \times (\boldsymbol{j} \times \boldsymbol{B})$ over the volume of the fluid is

$$\log 8 K c^{-4}((\zeta_0^2+1)^{\frac{1}{2}} - 1)\, \boldsymbol{e}_\phi. \tag{34}$$

Clearly (33) and (34) are decreasing functions of ζ_0, and this is the main reason for the reduction in the intensity of the flow field as ζ_0 decreases from 100 to 0.5. The reduction in u as ζ_0 decreases, that is as the electrode radius $k = c/\zeta_0$ increases, is in qualitative agreement with experiment, for example by Woods & Milner (1971). They passed various electric currents between two electrodes having diameters 3 mm and 15 mm respectively, which were immersed in a mercury bath. Along the axis the fluid was moving from the smaller to the larger electrode. When they repeated the experiment with the diameter of the smaller electrode doubled the observed maximum axial velocity at any given current was about halved. We note that at a given z the upper limit of u, for a particular K, is associated with the case of a point electrode (in a hemispherical container). In the case of the Stokes-flow regime for $z \geqslant 0.1$, the u corresponding to the point electrode (Sozou & Pickering 1976) is larger than the u corresponding to the case $\zeta_0 = 100$ by less than 5%.

We also note that, when $\zeta_0 = 1$ or $\zeta_0 = 0.5$, that is when the radius of the electrode k is comparable to the depth c of the container, the maximum value of u occurs approximately halfway up the axis (around $z = 0.5$) but when ζ_0 increases (and k decreases) the value of z where u becomes maximum decreases. Indeed when $\zeta_0 \to \infty$ and $k \to 0$, u becomes infinite at the origin. The position of the maximum of u for small k is in qualitative agreement with the experiments of Wienecke (1955) and Butsenieks *et al.* (1976). Wienecke determined the velocity field induced by a 200 A carbon arc. Along the axis of symmetry the flow field was directed from the small cathode to the larger anode. The observed maximum value of u was close to the cathode and exceeded 300 m s^{-1}. The values of u at 1.5, 2 and 2.5 cm from the cathode were 240, 180 and 120 m s^{-1}, respectively, and near the anode u was about 10 m s^{-1}. Butsenieks *et al.* studied the axisymmetric fluid motions generated in a closed cylindrical container filled with mercury. The height and radius of the container were both 15 cm, and the radii of the electrodes, which were attached to the plane ends of the cylinder, were 75 mm and 6 mm respectively. These authors noted that for the currents used u was proportional to J_0^2 and its maximum value occurred very close to the smaller electrode. (Their diagram 3(*a*) indicates that the maximum value of u occurs at a distance from the smaller electrode approximately equal to its radius.)

The effect of ζ_0 on the nonlinear u can be seen by considering the data for the two extreme values of ζ_0 shown in tables 1 and 2, namely $\zeta_0 = 100$ and $\zeta_0 = 0.5$. It is evident from table 1 that when $\zeta_0 = 100$, that is when the electrode size is small as K increases, u grows at a faster rate than K, especially near the boundary $z = 1$. The data of table 2 show that when $\zeta_0 = 0.5$, that is when the electrode size is large, u grows at a slower rate than K, except near the boundary $z = 1$, where initially u grows a little faster than K, but at sufficiently high K the growth of u is slower than that of K everywhere. As one might expect when $\zeta_0 = 10$ or $\zeta_0 = 1$ the behaviour of u, as K increases, lies between that for the two extreme cases of $\zeta_0 = 100$ and $\zeta_0 = 0.5$. When $\zeta_0 = 10$, for instance, as K increases, u/K decreases near $z = 0$ and increases near $z = 1$. The behaviour of u for the case $\zeta_0 = 10$ is qualitatively similar to that found by Atthey (1980, his table 1), though he considered a model different from the one employed here.

Details of the structure of the velocity fields for the cases $\zeta_0 = 100$, 1 and 0.5 respectively are shown in figures 2, 3 and 4. The asterisk shows the position of ψ_m, the maximum value of ψ, and we found that as K increases the position of ψ_m is pushed deeper into the container for all ζ_0 considered. The quantity $2\pi\psi_m$ represents the total volume flow generated by the discharge and is a measure of the overall intensity of the respective flow field. For the case $\zeta_0 = 100$, that is for the case of a

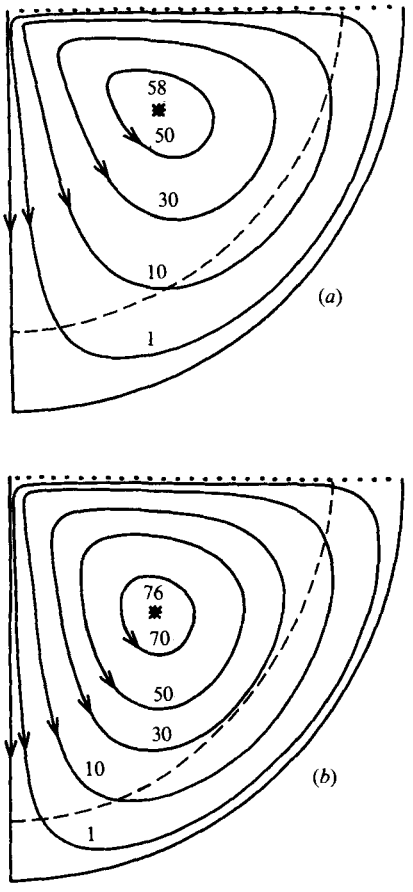

FIGURE 2. Meridional section of the flow field for the case $\zeta_0 = 100$: (*a*) linear case; (*b*) $K = 80$. The numbers on the curves are values of $10^4\psi/vcK$. The * shows the position where ψ is maximum. The broken curves separate the regions of oppositely directed (azimuthal) vorticity. The dotted lines represent the free surface.

small electrode, ψ_m/K increases as K increases, as evident from figure 2. This is in agreement with the case of a point electrode (in a hemispherical container) that was considered by Sozou & Pickering (1976). Our computations for $\zeta_0 = 1$, up to $K = 10^5$, and for $\zeta_0 = 0.5$, up to $K = 10^6$, show that ψ_m/K is approximately a constant. Details of our computer output reveal that the flow fields for $\zeta_0 = 1$ and for $\zeta_0 = 0.5$ are practically linear up to $K = 5 \times 10^3$ and $K = 5 \times 10^4$ respectively, but the flow fields for $\zeta_0 = 1$, $K = 10^5$ and $\zeta_0 = 0.5$, $K = 10^6$, as might be inferred from streamlines of figures 3 and 4 and the data of table 2, are nonlinear. For $\zeta_0 = 1$ we also constructed a solution for $K = 5 \times 10^5$, but that solution does not quite satisfy the condition $F_1(z) \gg |F_7(z)|$ for all z. For some z, F_1 was only slightly larger than $2|F_7|$. Also $|F_3(z)|$ was comparable to $F_1(z)$ and, for $z > 0.87$, $F_5(z) > F_1(z)$. This suggests that for the case $\zeta_0 = 1$, $K = 5 \times 10^5$, for an accurate representation of ψ, an N higher than 7 should be used and indicates that for $\zeta_0 = 1$ when K is 5×10^5 it is close to the limiting value beyond which the series (15) diverges. Also computations for $\zeta_0 = 0.5$ with a steplength $\delta z = 0.05$ show that the case $K = 2 \times 10^6$ will converge to a solution such that $F_1(z) \gg |F_{12}(z)|$, but the case $K = 4 \times 10^6$ is unstable and will not converge. When $\zeta_0 = 10$, ψ_m/K is 0.0040 for the linear problem and, when $K = 500$ and 1000, ψ_m/K

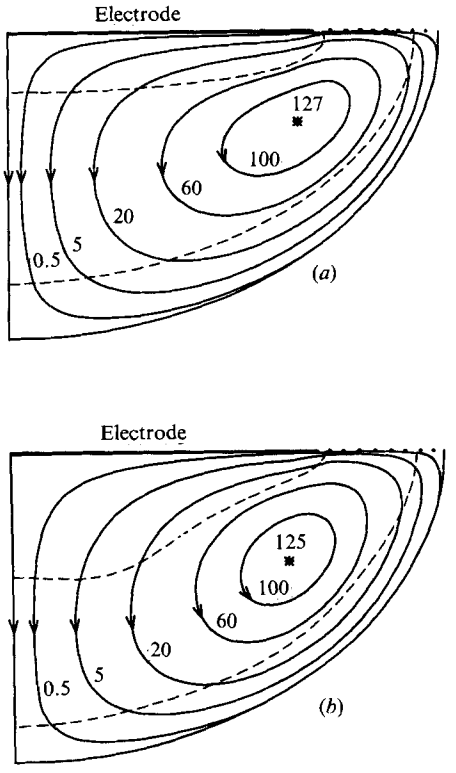

FIGURE 3. Meridional section of the flow field for the case $\zeta_0 = 1$: (*a*) linear case; (*b*) $K = 10^5$. The numbers on the curves are values of $10^6\psi/\nu cK$. The * shows the position where ψ is maximum. The broken curves separate the regions of oppositely directed (azimuthal) vorticity. The dotted lines represent the free surface.

is 0.0034 and 0.0027 respectively; that is, as K increases, the parameter ψ_m/K does not follow the pattern that one might expect from its behaviour for $\zeta_0 = 100$, 1 and 0.5. For $\zeta_0 = 10$, as K increases, the behaviour of ψ_m/K, like that of u mentioned earlier, is qualitatively similar to that noted by Atthey, who employed a model different from that used here.

The vorticity, given by (23), is azimuthal, and in the absence of solid boundaries, for the type of discharge considered here where the electric current diverges from a base at the plane boundary, it is in the positive ϕ-direction. The hemispheroid and electrode surfaces induce vorticity in the negative ϕ-direction and thus decrease the intensity of the flow field. The total vorticity near these surfaces is directed in the negative ϕ-direction, and in the intermediate region it is directed in the opposite sense. The broken curves of figures 2–4 separate the regions of oppositely directed vorticity. It is evident from these figures that, for a particular ζ_0, as K increases the intermediate region, where the vorticity is directed in the positive ϕ-sense, undergoes an overall contraction near the electrode and overall expansion near the surface of the container.

SP, using a different procedure for computing $F_n(z)$, found that, when $\zeta_0 < 0.65$, vortices develop at the electrode rim. Our method here did not show up these vortices. When one of us (O. O. A.) used a slightly different procedure for the evaluation of $F_n(z)$, these vortices were present; but, as K and the nonlinearities of the problem increase, the vortices become smaller and eventually disappear. However, owing to an oversight that program has been destroyed. It is probable that the vortices are there

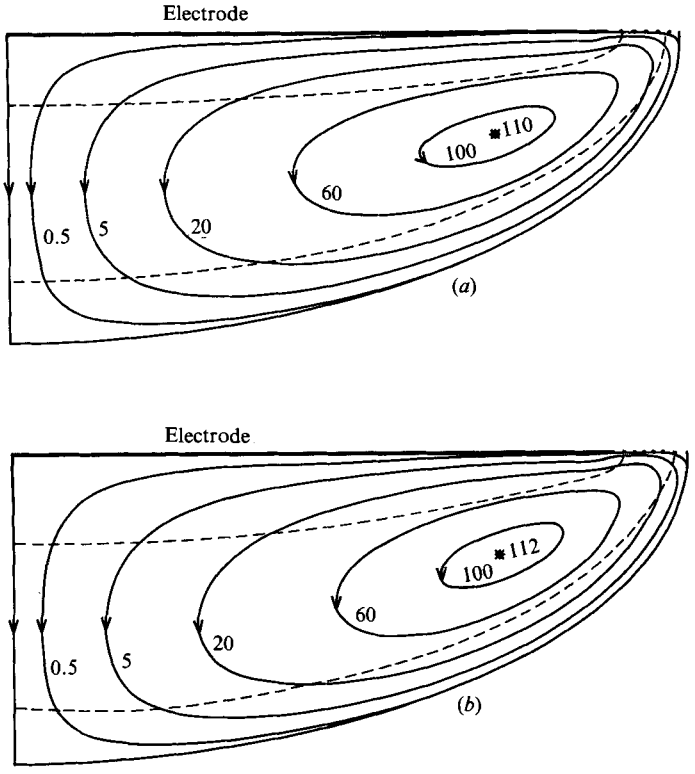

FIGURE 4. Meridional section of the flow field for the case $\zeta_0 = 0.5$: (*a*) linear case; (*b*) $K = 10^6$. The numbers on the curves are values of $10^7\psi/\nu cK$. The * shows the position where ψ is maximum. The broken curves separate the regions of oppositely directed (azimuthal) vorticity. The dotted lines represent the free surface.

and their detection depends on the refinement and accuracy of the method used to evaluate $F_n(z)$.

From the discussion so far it is evident that the geometry of the discharged current plays a major role in the quantitative determination of the velocity field. Indeed, for a specified container, by adjusting the size of the electrode (that is, the structure of the discharge), we can, for the same current and fluid, generate velocities that differ by several orders of magnitude. Therefore we cannot expect quantitative agreement between the experimental results and those of the above analysis, since, invariably, the geometry of the experiments conducted is different from that of the model used here. The results presented here, however, like those of previous studies, are in qualitative agreement with observation and demonstrate the importance of the structure of the discharge. Nevertheless, it would be instructive to insert in our parameters typical values of the data used in experimental and practical applications. In SI units $\chi = 4\pi \times 10^{-7}$ kg m s^{-2} A^{-2} and for steel welding $\nu = 10^{-6}$ m^2 s^{-1}, $\rho = 8 \times 10^3$ kg m^{-3}. Thus $J_0^2 = 0.126K$ A^2, and, when $J_0 = 100$ A, $K = 8 \times 10^4$. The case $\zeta_0 = 1$ of table 2 suggests that it is reasonable to assume that, for this K, the maximum value of $cu/\nu K \approx 3 \times 10^{-4}$. For a weld pool corresponding to $c = 0.0025$ m, $u \approx 0.01$ m s^{-1}. If the electrode size is smaller than c, u will be larger and *vice versa*. For mercury $\nu = 1.1 \times 10^{-7}$, $\rho \approx 1.4 \times 10^4$ and thus $J_0^2 \simeq 0.0026K$ A^2. If $J_0 = 100$ A then $K = 4 \times 10^6$. According to our computations there is velocity breakdown for this

case unless $k > 2c$, that is unless the container is very shallow. It may be of some relevance that the flow field observed by Woods & Milner (1971) in a mercury bath was turbulent even for currents of 50 A.

The analysis presented here is based on the assumption that the free surface is flat and thus the solution constructed is valid provided that the deviation of the free surface from the flat position is small. For the Stokes-flow problem the maximum deviation of the free surface can be worked out by the technique employed by SP, and it can be shown that for a weld pool of 2.5 mm it is small. Calculation of the deformation for the nonlinear problem is rather involved and has not been pursued, but, according to estimates by Craine & Weatherill (1980), the maximum deformation for this case, for the sort of currents considered here, is less than $0.1c$.

Appendix A

The functions $a_1, \ldots, a_{11}$ mentioned in §2 are defined as follows:

$$a_1 = \frac{z^2+\zeta_0^{-2}}{2n(2n+1)}\left(\frac{\zeta_0^2 z^2}{4n+1}+\frac{8n^2+4n-3}{\alpha(n)}\right), \quad a_2 = -\frac{2z(\zeta_0^2 z^2+1)}{n(2n+1)(4n+1)},$$

$$a_3 = -\frac{(n-1)(2n+3)\zeta_0^2 z^2-2}{n(2n+1)(4n+1)} - \frac{(8n^2+4n-3)(2n^2+n+2)-3}{n(2n+1)\alpha(n)},$$

$$a_4 = \frac{z^2+\zeta_0^{-2}}{\alpha(n+\frac{1}{2})}, \quad a_5 = -\frac{4n^2+18n+20}{\alpha(n+\frac{1}{2})}, \quad a_6 = \frac{z^2+\zeta_0^{-2}}{\alpha(n-\frac{1}{2})},$$

$$a_7 = -\frac{4n^2-14n+12}{\alpha(n-\frac{1}{2})}, \quad a_8 = (\zeta_0^2 z^2+1)c_1+c_2,$$

$$a_9 = -2\zeta_0^2 z\left(2c_1+\frac{c_2}{\zeta_0^2 z^2+1}\right), \quad a_{10} = (\zeta_0^2 z^2+1)c_3+c_4,$$

$$(\zeta_0^2 z^2+1)a_{11} = \begin{cases} \frac{1}{12}z(\zeta_0^4 z^4+\frac{3}{5}\zeta_0^2 z^2+\frac{1}{7}) & (n=1), \\ -z(\frac{3}{160}\zeta_0^4 z^4-\frac{1}{240}\zeta_0^2 z^2-\frac{13}{2752}) & (n=2), \\ -\dfrac{zP_{2n}(0)}{2n(2n+1)}\left(\zeta_0^4 z^4-\dfrac{2\zeta_0^2 z^2}{(n+1)(2n-1)}\right. & \\ \left.+\dfrac{6}{(n+1)(n+2)(2n-1)(2n-3)}\right) & (n \geqslant 3), \end{cases}$$

where

$$\alpha(n) = (4n-1)(4n+1)(4n+3),$$

$$c_1 = -\int_0^1 \frac{I_{2n+1}(x)\, I_{2s+1}(x)\, P_{2m}(x)}{1-x^2}\,\mathrm{d}x, \quad c_2 = \int_0^1 I_{2n+1}(x)\, I_{2s+1}(x)\, P_{2m}(x)\,\mathrm{d}x,$$

$$c_3 = \int_0^1 \left[-\frac{2xI_{2s+1}(x)}{(1-x^2)^2}+\frac{P_{2s}(x)}{1-x^2}\right] I_{2m+1}(x)\, I_{2n+1}(x)\,\mathrm{d}x,$$

$$c_4 = \int_0^1 \left[\frac{4xI_{2s+1}(x)}{1-x^2}-P_{2s}(x)\right] I_{2m+1}(x)\, I_{2n+1}(x)\,\mathrm{d}x.$$

Appendix B

The axisymmetric flow field generated by the discharge of an electric current J_0 in a semi-infinite fluid from a point at the plane interface of the fluid is given by (Sozou 1971)

$$\psi = \nu r g(\mu), \tag{B 1}$$

where

$$g = -2(1-\mu^2)\frac{u'(\mu)}{u(\mu)}, \tag{B 2}$$

$$u'' = \frac{Ku[a\mu^2+b+c-(1+\mu)^2\log(1+\mu)]}{4(1-\mu^2)^2}, \tag{B 3}$$

$K = \chi J_0^2/2\pi^2\nu^2\rho$, and a, b and c are constants. In this formulation spherical polars (r, θ, ϕ) are used and the origin is at the current source. The plane boundary of the fluid is given by $\theta = \frac{1}{2}\pi$, the axis $\theta = 0$ is directed into the fluid and $\mu = \cos\theta$.

When the plane boundary is a solid plate, where $v = 0$ (Sozou 1971), the constants a, b and c are given by

$$a = 2, \quad b = 4\log 2 - 2, \quad c = 0,$$

and when the plane boundary is a free surface, where v is tangential and the shear stress is zero (Sozou & Pickering 1976), the constants take the values

$$a = \tfrac{1}{2} + 2\log 2, \quad b = 1, \quad c = -\tfrac{3}{2} + 2\log 2.$$

The solution of (B 3) is subject to the conditions $u'(0) = 0$ and $u(0) =$ constant, say $u(0) = 1$.

Equation (B 3) was solved numerically (Sozou 1971; Sozou & Pickering 1976) by marching forward from $\mu = 0$ to $\mu = 1$. It was found that when K exceeds K_{crit}, where K_{crit} is a critical value, u has zeros in the range $0 < \mu < 1$ and thus ψ and v become infinite. The solutions associated with $K > K_{\text{crit}}$ are not physically meaningful.

The solution of (B 3) can also be constructed in terms of power series. The coefficient of u on the right-hand side of (B 3) can be expanded as a power series about the point $\mu = 1$; this expansion is

$$\sum_{n=0}^{\infty} a_n(1-\mu)^n,$$

where

$$a_n = (\tfrac{1}{2})^{n+5} K\left[n-1+\frac{2}{n+2}+(n+1)C\right],$$

where $C = 1-2\log 2$ when the plane boundary is a solid plate and $C = 2\log 2 - 2$ when the plane boundary is a free surface. It can then be shown that the two solutions, say u_1 and u_2, of (B 3) are given by

$$u_1 = \sum_{n=0}^{\infty} b_n(1-\mu)^n, \quad u_2 = \sum_{n=1}^{\infty} c_n(1-\mu)^n, \tag{B 4), (B 5}$$

where $b_0 = 1$, $b_1 = 0$, $c_1 = 1$, $c_2 = 0$ and the remaining bs and cs are given by

$$b_n = \frac{1}{n(n-1)}(a_0 b_{n-2} + a_1 b_{n-3} + \ldots + a_{n-2} b_0),$$

$$c_n = \frac{1}{n(n-1)}(a_0 c_{n-2} + a_1 c_{n-3} + \ldots + a_{n-3} c_1).$$

We have computed several coefficients b_n and c_n for values of K up to 5000, and our computations indicate that, in the range $0 < \mu < 1$, u_1 and u_2 converge for *all* K. As K increases, the number of terms needed in order to obtain an accurate representation for u_1 and u_2 increases slowly, but for values of K up to K_{crit} a moderate number of terms provides a reasonably accurate evaluation for u_1 and u_2. (When $K \approx K_{\text{crit}}$, b_{10} and c_{10} are $O(10^{-4})$, b_{16} and c_{16} are $O(10^{-5})$ or less, and, for $n \geqslant 16$, $|b_{n+1}/b_n|$, $|c_{n+1}/c_n| < 0.6$.)

If we set

$$u = A_1 u_1 + u_2, \tag{B 6}$$

the condition $u'(0) = 0$ implies $A_1 = -u_2'(0)/u_1'(0)$. Our computations showed that, for $K < K_{\text{crit}}$, $A_1 > 0$, and, as K increases, A_1 decreases; K_{crit} is the value of K that satisfies the condition $A_1 = u_2'(0) = 0$. Since $\boldsymbol{v}\cdot\boldsymbol{r} = -\nu g'/r$, (B 2) and (B 4)–(B 6) imply that, when $A_1 = 0$, $\boldsymbol{v}$ is infinite on $\mu = 1$. As with the numerically constructed solutions we find that $K_{\text{crit}} \approx 300.1$ when the plane $\mu = 0$ is a solid plate, and $K_{\text{crit}} \approx 94.1$ when the plane $\mu = 0$ is a free surface. When $K > K_{\text{crit}}$, u has zeros in the range $0 < \mu < 1$, i.e. ψ and $\boldsymbol{v}$ have singularities and the behaviour of the solution as K increases gradually beyond K_{crit} is exactly as described by Sozou (1971).

REFERENCES

Andrews, J. G. & Craine, R. E. 1978 *J. Fluid Mech.* **84**, 281.

Apps, R. L. & Milner, D. R. 1963 *Brit. Weld. J.* **10**, 348.

Atthey, D. R. 1980 *J. Fluid Mech.* **98**, 787.

Boyarevich, V. 1981 *Magnetohydrodyn.* **17**, 141 (English transl.).

Boyarevich, V. & Shcherbinin, E. V. 1983 *J. Fluid Mech.* **126**, 413.

Butsenieks, I. E., Peterson, D. E., Sharamkin, V. I. & Shcherbinin, E. V. 1976 *Magnetohydrodyn.* **12**, 70 (English transl.).

Christensen, N., Davis, V. de L. & Gjermundsen, K. 1965 *Brit. Weld. J.* **12**, 54.

Craine, R. E. & Weatherill, N. P. 1980 *J. Fluid Mech.* **99**, 1.

Kublanov, V. & Erokhin, A. 1974 *Intl Inst. Weld. Doc.* 212-318-74.

Lamb, H. 1932 *Hydrodynamics.* Cambridge University Press.

Lundquist, S. 1969 *Ark. Fys.* **40**, 89.

Milner, D. R., Salter, G. R. & Wilkinson, J. B. 1960 *Brit. Weld. J.* **7**, 73.

Shercliff, J. A. 1970 *J. Fluid Mech.* **40**, 241.

Sozou, C. 1971 *J. Fluid Mech.* **46**, 25.

Sozou, C. 1974 *J. Fluid Mech.* **63**, 665.

Sozou, C. & Pickering, W. M. 1976 *J. Fluid Mech.* **73**, 641.

Sozou, C. & Pickering, W. M. 1978 *Proc. R. Soc. Lond.* A **362**, 509.

Wienecke, R. 1955 *Z. Phys.* **143**, 128.

Woods, R. A. & Milner, D. R. 1971 *Weld J.* **50** (Res. Suppl.), 163.